Physica A 537 (2020) 122679

Contents lists available at ScienceDirect

Physica A

journal homepage: www.elsevier.com/locate/physa

Atomistic model derived from ab initio calculations tested in Benzene–Benzene interaction potential

Elizane Efigenia de Moraes [a,*], Mariana Zancan Tonel [a], Solange Binotto Fagan [b], Marcia C. Barbosa [a]

[a] Instituto de Física, Universidade Federal do Rio Grande do Sul, Porto Alegre, RS 91501-970, Brazil
[b] Centro de Ciências Naturais e Tecnológicas, Universidade Franciscana, Santa Maria, RS 97010-032, Brazil

ARTICLE INFO

Article history:
Received 23 April 2019
Received in revised form 19 August 2019
Available online 14 September 2019

Keywords:
Benzene
Quantum mechanics
Atomistic potentials
Molecular dynamics simulations

ABSTRACT

We employ ab initio Density Functional Theory to develop classical atomistic potentials. We test this method developing a novel benzene–benzene atomistic model parameterized through quantum mechanical approach with no experimental data fitting. Thermodynamic and dynamic properties of the effective model were derived using molecular dynamic simulations. The diffusion coefficient and activation energies were computed showing results consistent with the experiments. The model also provides a very good representation of the three peaks of molecular orientations for benzene liquid. The simplicity of the model allow us to suggest mechanisms for the orientation and mobility of the molecules.

1. Introduction

Computer simulations are a very important tool to describe molecular systems of solutions in the bulk or under confinement. This technique not only can explore regions of pressure and temperature difficult to be reached by experiments but also provides a way to test which interactions are relevant in a determinate system at a specific state. The possibility of building potentials as a combination of different interactions allows for the discovery of the mechanism behind a certain property or behavior. However, the key part of the simulations is the construction of the force field. The most employed strategy is the atomistic approach in which a priori potential for the atoms interaction is proposed. In this case the force field parameters are adjusted to reproduce a set of macroscopic experimental properties at a fixed temperature or pressure. The potential created in this way contains the many body interactions inside the two body potential. Even though this procedure has been quite successful in describing certain properties of molecular system, it fails to predict others.

In principle complex force fields, with a large number of parameters, should exhibit a better performance. This, however, is not always the case. Attempts to create a force field for water have generated more than 35 models some of then with 3, 4, 5 or even 6 sites of interaction. Even though more sites correspond to larger number of parameters what in principle could optimize the model, the four sites Tip4p/ϵ show the best performance [1,2]. Another particular case are the polarizable models [3] which present a parameter optimization procedure very computationally cost. These models [4] are also very important because even thought now able to obtain a number of thermodynamic quantities properly they are the only models capable to give the increase of the water diffusion with the increase of salt concentration observed

* Corresponding author.
E-mail address: elizane.fisica@gmail.com (E.E. de Moraes).

https://doi.org/10.1016/j.physa.2019.122679
0378-4371/

experimentally [5]. Therefore, the diversity of models helps in understanding which interactions are more relevant what might change with temperature, pressure, confinement and mixtures.

Complementary to the atomistic fitting method, another possible approach is to construct a force field from first principles. While the atomistic approach fits the parameters with room temperature experimental quantities which captures the average configuration, the first principles focus on the zero temperature configurations what captures the minimum energy configurations. The idea is to use quantum mechanical calculations for a set of representative intermolecular geometries which will be used in simulations. This ab initio quantum mechanics calculation as the number of particles increase quickly becomes not computationally feasible. In order to circumvent this difficulty one strategy is to select only a few lower energy configurations and construct a two body interaction on basis of these elements [6]. The quantum mechanics is implemented through Density Functional Theory (DFT) [7]. Since for each system different functionals have been implemented, the quantum method can also present a diversity of models.

Here we propose that even though the selection of the quantum mechanical functional in the ab initio approach affects the quantitative value of the energy of the system, since most functionals agree about which configurations exhibit the minimum energy, the final potential employed in the molecular dynamic simulations give very similar molecular structure. We argue that the strength of developing a model based in DFT is not to provide a correct value for the density or the pressure of the system (usually well capture by the atomistic approach) but to give understanding of the origin of the observed molecular structure computed by the radial distribution function. Here we test this assumption by creating a minimum pair potential for the benzene–benzene interaction. The relevant question is if this effective potential like the potential employed in liquid water [8] is capable to describe the pair potential in terms of the benzene molecular local orientation which origin seems to be still under some debate [6,9–18].

Experiments using X-ray diffraction [9] and scattering [13,15] show structure at the liquid phase. In parallel, results with neutron diffraction [19,20] and X-ray scattering [13,15] using deuterated benzene show less structure since they only produce the intermolecular radial distribution function and not the carbon–carbon distribution function. The X-ray diffraction shows that the liquid structure of benzene at 25 °C is similar to that found in the crystalline state. In addition the carbon–carbon intermolecular pair distribution function (RDF) exhibits three peaks of carbon–carbon intermolecular orientation for benzene. The physical explanation of the location of the peaks is still under debate. It is attributed either to the organization of the liquid in preferential arrangements, either a T-Shaped carbon–carbon intermolecular orientation [9] or a T-Shaped displaced [13] or even a parallel displaced arrangement of the molecules [21].

Many classical molecular dynamic (MD) [6,10,14,18,19] and Monte Carlo (MC) [12,22–24] have been performed on liquid benzene using various intermolecular potentials. The idea behind these models is that they propose a potential interaction with a combination of attraction, hardcore and electrostatics which are parameterized employing experimental results at room temperature and pressure. The simplest versions of this models use only a Lennard-Jones potential [10,24]. These atomistic potentials are able to reproduce a number of state variables such as the density at different temperatures and pressures around the value for which they were parameterized. However, they are not able to capture of the three peaks molecular orientations of RDF for benzene. More complex models [10,14,25] reproduce the three peaks but not the relative position and height of the peaks. This information would be quite important to determine if the preferential arrangement of the molecules is perpendicular shaped as proposed by the experiments [9,13].

Here we attempt to understand the structure of benzene by deriving an effective interaction potential from ab initio calculations. The idea behind the analysis is that by employing quantum calculations some of the ground state structure will be capture by our potential. The remaining of the paper goes as follows. In Section 2 the computational details of the ab initio calculations, the employed model potential and the simulations techniques are presented. In Section 3 the results and discussion are analyzed and conclusions are presented in Section 4.

2. Model and methods

2.1. Quantum calculations

We obtained the energies of two benzene molecules for various distances and orientations between the molecules. The energies were calculated within the framework of density functional theory (DFT) [26–28], as implemented in the SIESTA (Spanish Initiative for the Electronic Simulations of Thousands of Atoms) code [29]. The electronic, energetic and structural properties were analyzed solving the self-consistent Kohn–Sham equations [27]. In all calculations, a double ζ plus a polarized function (DZP) was used for the numerical basis set. In order to describe the exchange and correlation potential (V_{xc}) we investigated the performance of the three functional implemented in the SIESTA: (i) the Local Density Approximation (LDA) with the Perdew and Zunge (PZ) parametrization [30] the correction to basis set superposition error (BSSE-corrected) [31], (ii) the Generalized Gradient Approximation (GGA) with the Perdew, Burke and Ernzerhof (PBE) version [32], and (iii) and GGA dispersion correction [33] with the Perdew, Burke and Ernzerhof (PBE) version [32,34].

In this work we adopt the LDA functional with the correction to basis for two complementary reasons. First, when compared with the other options listed above, it gives a better agreement with the literature [6,18,35,36] for the minimum energies configuration. The second reason is that for the calculation of the effective potential the energy has to go to zero at distances above 4 Å . This is only the case for the case LDA with correction to basis.

In order to represent the electronic charge in real space, a grid cutoff of 200Ry was used. All of the studied systems present a neutral charge in the initial electronic configuration. The BZ–BZ interaction we use a super cell of $(40 \times 40 \times 40)$

Table 1
Configuration k, distance minimum r_0, and maximum r_{cut} for the calculated the interaction energies between benzene dimers.

Configurations K	r_0 (Å)	r_{cut} (Å)
(a) Side by Side	1.0	4.0
(b) T-Shaped	1.0	4.0
(c) T-Shaped Displaced	1.0	7.0
(d) Face to Face	2.4	6.0
(e) Slipped Parallel	1.8	5.0

Å^3. The relative numerical accuracy on the interaction energy computed with the correction to basis set superposition error (BSSE-corrected) is estimated to be of the order of around 0.96 kJ/mol. The isolated molecules are relaxed residual forces lower than 0.05 eV/Å and then kept rigid the interactions of the homodimers and the molar mass of benzene is 78.1118 g/mol. The distance (r) between the benzene dimers refers to the minimum atom–atom distance of each configuration studied. We selected five configurations for the benzene–benzene interactions. This selection is based on the distribution of charges in valence band maximum and conduction band minimum. In this case, we observed that the charge on both the VBM and CBM is evenly distributed in the ring aromatic carbons, indicating that it is the most favorable site for the interactions [9,19,37,38] . The distance minimum, r_0 and maximum, r_{cut} is shown for each configuration in the Table 1.

The interaction energies between benzene dimers for a given configuration k and distance $r_0 \leq r \leq r_{cut}$ were calculated using the correction to basis set superposition error (BSSE-corrected) [31] by the following equation:

$$E_k(r) = E_k^{AB}(r) - E_k^{A,ghostB}(r) - E_k^{ghostA,B}(r), \tag{1}$$

where E_{AB} is the total energy of benzene dimer, $E_A^{ghostB}(E_B^{ghostA})$ is the total energy of part isolated A (B). The part A corresponds to monomer benzene, and part B is other monomer benzene. They were calculated with their corresponding atomic basis and with the A (B) atomic basis centered at the B (A) atomic positions. The subscript ghost refers to the atomic basis placed on the monomer benzene or other molecule positions but without atomic potentials representing real atoms at these positions and of the system with negative binding energies implies attractive interaction.

2.2. Intermolecular potential parametrization

For the effective potential, each benzene is a rigid molecule formed by six sites. The sites are distant from each other 1.41 Å. The intermolecular interaction was modeled by each atom of one molecule interacting with each atom of the other molecule by a modified version of 12–6 Lennard-Jones (LJ) defined as [39]

$$u_{ij}\left(r_{ij}\right) = \epsilon \left[\left(\frac{\xi_{ij}\sigma_{ij}}{r_{ij} - \left(\xi_{ij} - 1\right)\sigma_{ij}} \right)^{12} - \left(\frac{\zeta_{ij}\sigma_{ij}}{r_{ij} - \left(\zeta_{ij} - 1\right)\sigma_{ij}} \right)^{6} \right], \tag{2}$$

where i and j are atomic index for two monomers belonging to different dimers, $r_{ij} = |\boldsymbol{r}_i - \boldsymbol{r}_j|$ is the distance between sites i and j. The parameters σ_{ij}, and ϵ_{ij} represent the van der Waals length and depth, respectively. The parameters ξ_{ij} and ζ_{ij} are auxiliary variables in which are added to improve the flexibility of the potential to the ab initio data. Here, the ζ and ξ allow the attractive and repulsive part to have decoupled distance scales which is reasonable, since the repulsion is governed by the nuclear core, while the attractive part is related to the electron cloud. The 12-6 LJ force field are re-parameterized to reproduce the QM intermolecular interactions. For a given configuration and distance between the two dimers, the total potential energy becomes

$$U_k(\boldsymbol{A}) = \sum_{i=1}^{6}\sum_{j=1}^{6} u_{ij}\left(r_{ij}\right), \tag{3}$$

where $\boldsymbol{A}$ represents the set of parameters $\boldsymbol{A} = \{\sigma, \epsilon, \xi, \zeta\}$.

Next, the parameters of the effective potential, $\boldsymbol{A} = \{\sigma, \epsilon, \xi, \zeta\}$ are adjusted to give the best fit with the density functional energies of the different configurations and distances following the methodology proposed by the Cacelli et al. [18,40–42]. The numerical procedure consists in a nonlinear minimization routine. We have used the Sequential Least Squares Programming (SLSQP) from `optimize.scipy` [43,44] to minimize the function

$$I(\boldsymbol{A}) = \left(\sum_{k=1}^{Ng} \omega_k \right)^{-1} \sum_{k=1}^{Ng} \sum_{r=r_0}^{r_{cut}} \omega_k \left[E_k(r) - U_k\left(\boldsymbol{A}, r\right) \right]^2, \tag{4}$$

where E_k is the energy obtained for the DFT, r is the distance between refers to the minimum atom–atom distance of each configuration studied and Ng is the number of geometries considered and r_0 and r_{cut} are the minimum and maximum distances between the minimum atom–atom distance of each configuration of the two dimers computed in the DFT. The index, k, specifies the geometry of benzene dimer, and the $\omega_k = \exp\left(-k_B E_k\right)$ weight of the configuration with the Boltzmann factor.

2.3. Molecular dynamics calculations

Molecular dynamics simulations in the NVT ensemble were performed for the benzene modeled as six-site molecules. The intermolecular potential u_{ij} employed is described by Eq. (2) and the parameters obtained by the optimization. The effective potential is illustrated in dimensionless units in Fig. 3, We employed N = 125, 209, 417, 625, 1042 molecules in a cubic box of volume V with periodic boundary conditions in the three directions. The simulations were implemented using the LAMMPS package [45] based on the constraint method to integrate the equation movement. The number density of the system is then = N/V. The cutoff radius was set to 3.5 σ. All simulations of the rigid models molecule were performed pressure, temperature, density, and diffusion are calculated in dimensionless units,

$$P^* = \frac{P\sigma^3}{\epsilon}, \tag{5}$$

$$T^* = \frac{k_B T}{\epsilon}, \tag{6}$$

$$\rho^* = \rho\sigma^3, \tag{7}$$

$$D^* = \frac{D(\frac{m}{\epsilon})^{0.5}}{\sigma}, \tag{8}$$

where $\sigma^* = \epsilon^* = 1$ and $m^* = 1$. After a equilibration time of 10^7 steps, the thermodynamic, structural and dynamic properties were calculated using 4×10^7 simulation steps where providing instant settings for every 4000 steps, giving a total of 10 000 independent settings. The time step was 0.001 in reduced units and the time constant of the Nosé–Hoover thermostat [46,47] 1 in reduced units. The internal bonds between the particles in each dimer remain fixed using the rigid package [45].

The stability of the system was checked by analyzing the dependence of pressure on density and also by visual analysis of the final structure, searching the potential energy versus runs. The structure of the system was calculated using the intermolecular radial distribution function, $g(\vec{r})$ (RDF), which does not take into account the correlation between atoms belonging to the same molecule. The diffusion coefficient was calculated using the slope of the least square fit to the linear part of the mean square displacement, $\langle r^2 \rangle$ (MSD), were computed taking the origin as the center of mass of a dimer.

The Radial Distribution Function (RDF), $g_{\alpha,\beta}(r)$ between the carbon α of one molecule and the β belonging to another was computed by:

$$g_{\alpha,\beta}(r) = \frac{N_\alpha^{-1}}{\langle\rho\rangle_{local}} \sum_{i\in\alpha}^{N_\alpha} \sum_{j\in\beta}^{N_\beta} \frac{\delta(r_{ij} - r)}{4\pi r^2}, \tag{9}$$

in which ρ is the density. In our case we computed the intermolecular $g(r)$ for a fix atom of each molecule.

In order to study the mobility we employed the mean square displacement (MSD) given by

$$\langle (r(t) - r(0))^2 \rangle = \langle (\Delta r(t))^2 \rangle, \tag{10}$$

where $r(0)$ is the position of the carbon at one molecule at the time zero while $r(t)$ is the position at a time t. The mobility of the particles was averaged over all the carbons. When the molecules exhibit diffusive regime, we calculated the diffusion coefficient, D, from the slope of the plot of the MSD against time, as follows

$$D = \lim_{t\to+\infty} \frac{\langle (\Delta r(t))^2 \rangle}{2dt}, \tag{11}$$

where d is the dimension, $\langle \cdots \rangle$ denotes an average over molecules and time origins.

3. Results and discussion

3.1. Quantum energies and effective potential

First, we selected more favorable benzene–benzene configurations namely (a) Side by Side (SS), (b) T-Shaped (TS), (c) T-Shaped Displaced (TSD), (d) Face to Face (FF), and (e) Slipped Parallel (SP) as shown in the Fig. 1 and we obtained the DFT energies for different distances atom–atom between the dimer ranging from r_0 to r_{cut}. These energies as a function of the dimer distances are plotted in Fig. 2 as circles.

Within the DFT energies obtained for the different configurations, the T-Shaped and the T-Shaped Displaced configurations, illustrated in Fig. 2(b) and (c), present the lower minimum. The lower energy of the benzene–benzene

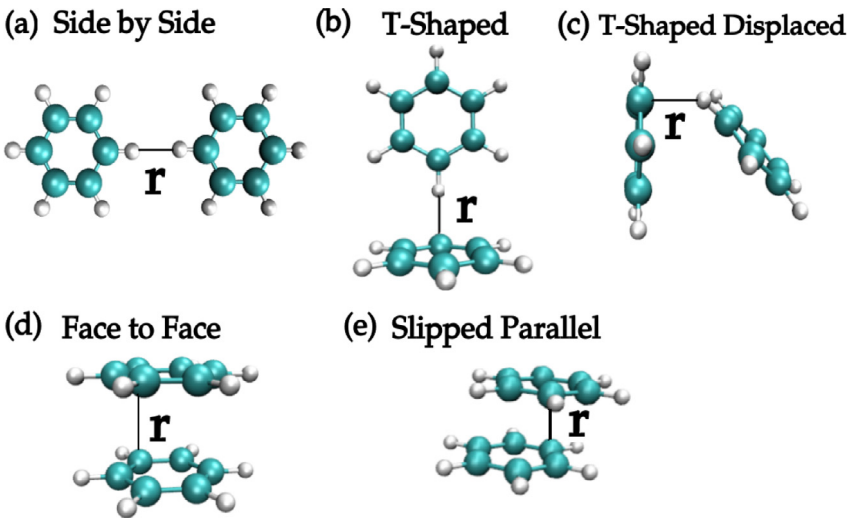

Fig. 1. Stacked benzene dimer: (a) Side by Side (SS), (b) T-Shaped (TS), (c) T-Shaped Displaced (TSD), (d) Face to Face (FF), and (e) Slipped Parallel (SP). C atoms are cyan and H atoms are white.

Table 2
DFT minimum energy E_{min} and value of the distance of this minimum value for the many different configurations.

Configurations	E_{min} (kJ/mol)	r_{min} (Å)
(a) Side by Side	−2.122677	2.0
(b) T-Shaped	−9.0	2.5
(c) T-Shaped Displaced	−7.2	2.25
(d) Face to Face	−2.97	3.75
(e) Slipped Parallel	−6.63	3.5

perpendicular orientation is also observed in results obtained employing other functionals [6,18] and is predicted by the experiments [9,13] and simulations [11].

The attractive behavior of the TS configurations can be explained by in terms of the favorable electrostatic interaction between the negatively charged π-cloud of the lower ring, and the positively charged hydrogen atom of the other ring above it. The minimum DFT energy , E_{min} and its location, r_{min}, is shown for each configuration in Table 2. The slipped parallel configurations show an increase of the attraction interaction energy when comparing the pure parallel. The pure aromatic interaction is dominated by the benzene–benzene quadrupole repulsion [16,48] while the displaced has a component of attraction induced by the exposed hydrogen.

The classic intermolecular potentials derived upon optimization for the (a) SS, (b) TS, and (c) DC configurations show smooth interpolations of quantum energies. This is not the case for the configurations (d) FF and (e) SP which show diverging potentials at small distances. The same effect was observed in other attempts to produce effective potentials for ab initio energies [18,40]. In order to circumvent this inconvenience in the derivation of a single potential to cover all the configurations, we started the parametrization at $r_0' = 2.5$ Å for the FF arrangement and $r_0' = 1.8$ Å for the SP configuration.

Then, in order to test if the procedure to produce an effective potential from the ab initio energies works, we computed the effective potential, U_k, for each k dimer configuration. The optimal values for $\boldsymbol{A} = \{\sigma, \epsilon, \xi, \zeta\}$ were determined to give the best fit for each E_k, where k represents each configuration. The resulting fit is shown in the Fig. 2 as a line. Table 3 shows the best Lennard-Jones parameters ($\boldsymbol{A} = \{\epsilon, \sigma, \zeta, \xi\}$) of the classical intermolecular potential for each isolated configuration of the dimers. The factor considering α parameter 3.47347 kJ/mol as in the Ref. [40] to privilege the small attractive part of each the configurations.

Next, the procedure described by Eq. (4) was implemented taking into account not one but all configurations weighting them by $\omega_k = e^{\alpha E_k}$. The weight factor $\omega_k = \exp(-\alpha E_k)$ favors the lower energy dimer configurations with the α parameter fixed in 3.47347 kJ/mol as in the Ref. [40]. In order to circumvent the diverging values at small distances for the (d) FF and (e) SP in the derivation of a single potential we start the parametrization at $r_0' = 2.5$ Å. The Fig. 3 shows the classical intermolecular potential between the site of one molecule and the site of the other molecule in reduced units for the benzene–benzene interaction, obtained after the minimization process described in the previous section.

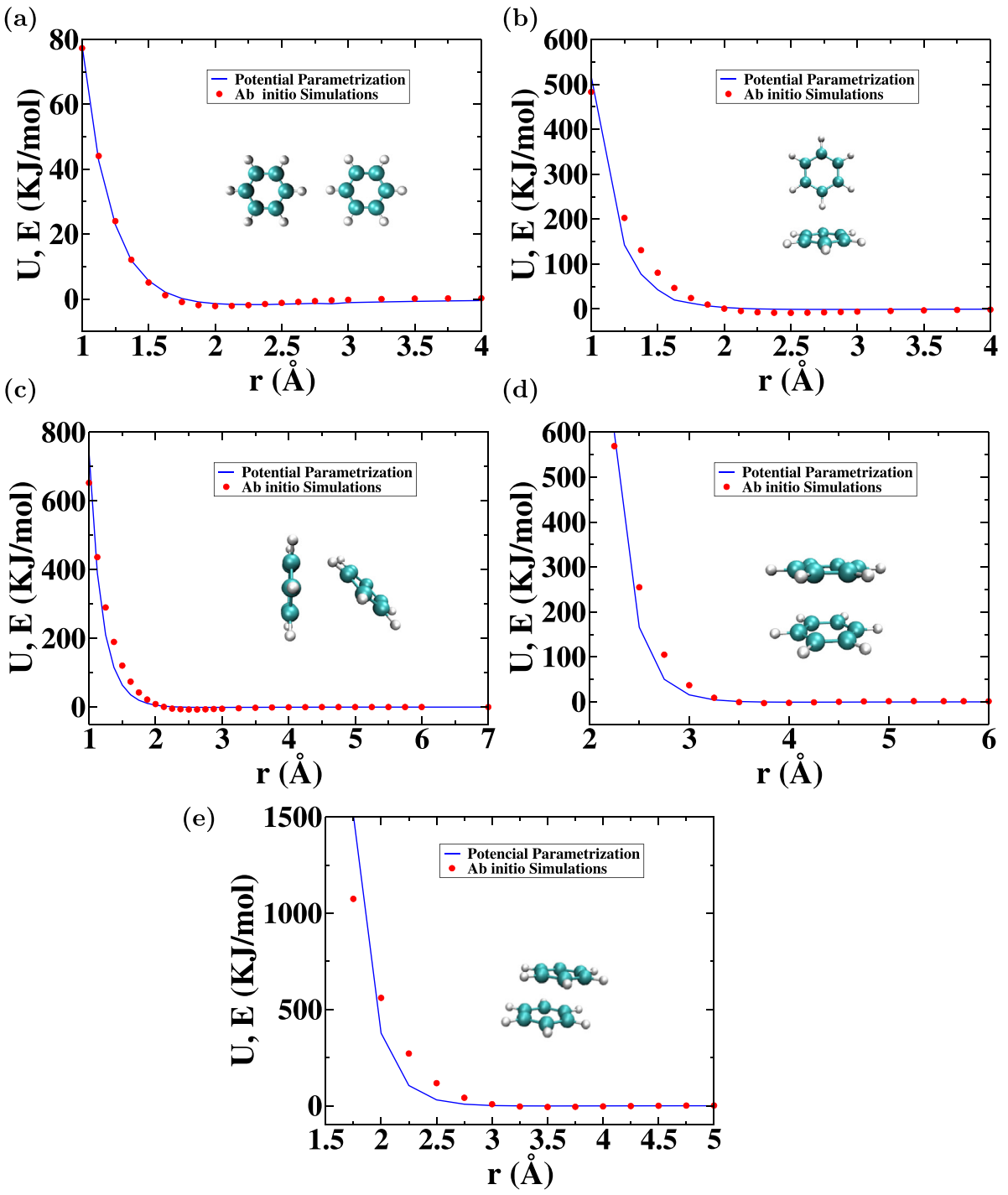

Fig. 2. Intermolecular energies for the benzene dimer in some typical arguments: blue curve parameterized intermolecular potential (U), and red curve ab initio energies (E).

3.2. Molecular dynamics results

We carried out a molecular dynamic simulations in the NVT ensemble of rigid benzene interacting with the potential derived from ab initio calculations, illustrated in Fig. 3. The system presents a number of structures including a very low density phase, gas-like, a high density liquid-like and a dense structure, solid-like.

Table 3
12–6 LJ fitted force fields parameters based on minimizing the function $I(\boldsymbol{A})$ of between intermolecular interaction from QM for each isolated configuration of the benzene dimers.

Configurations	ϵ (kJ/mol)	σ (Å)	ξ	ζ
(a) Side by Side	0.3538	3.815	1.129	1.171
(b) T-Shaped	0.27	3.9	1.0	1.0
(c) T-Shaped Displaced	0.212	3.764	1.0	1.0
(d) Face to Face	0.212	3.427	1.0	1.0
(e) Slipped Parallel	0.192	3.38	1.0	1.0

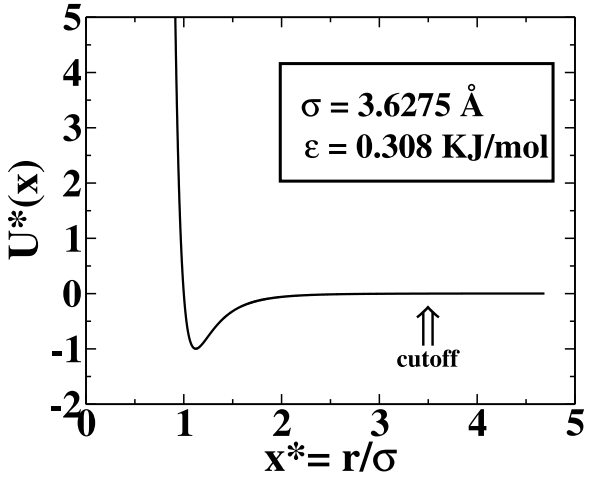

Fig. 3. Effective potential versus distance of the benzene derived from ab initio calculations, in reduced units.

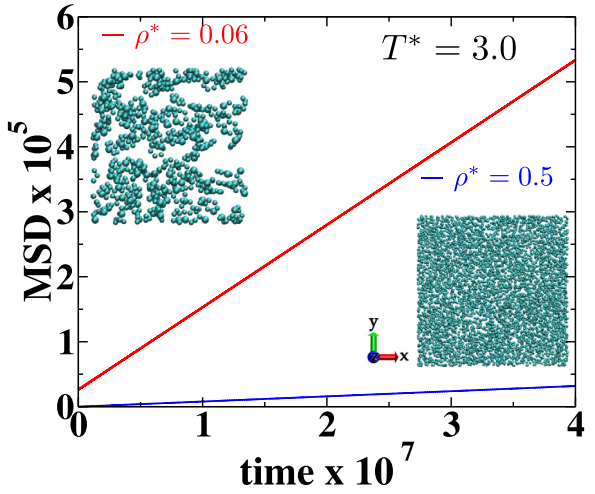

Fig. 4. The mean square displacement versus time and snapshots from $\rho^* = 0.06$ to $\rho^* = 0.5$ for fixed $T^* = 3.0$.

In order to identify the solid/amorphous and fluid structures we computed the mean square displacement given by the Eq. 4 for reduced temperatures $T^* = 2.5 - 5.0$ and reduced densities $\rho^* = 0.06, 0.1, 0.2, 0.3$, and 0.5. The Fig. 4 illustrates two extreme structures observed at $T^* = 3.0$: a fluid phase at low densities $\rho^* = 0.06$ and an amorphous phase at $\rho^* = 0.5$. They show a very dense solid/amorphous-like region at $T^* = 3.0$ and $\rho^* = 0.5$ and a fluid phase at $T^* = 3.0$ and $\rho^* = 0.06$. The fluid phase depicted by the snapshot shows the presence of cluster of molecules which at the very dense phase form a continuous structure. The formation of clusters at the fluid phase is consistent with experimental [49,50] and simulations [10–12,51–54] of more complex atomistic models. The cluster size depends on the temperature and density.

From all the MSD at the fluid phase we computed the diffusion coefficient employing the Eq. 5. The mobility of the particles decreases with the increasing density (or pressure) for constant temperature as shown in the Fig. 5 and as

Table 4
Density ρ^*, ρ and activation energy E_p obtained with our simple model derived from ab initio calculations for the benzene.

ρ^*	ρ (g/cm^3)	E_p (kJ/mol)
0.06	0.163	15.8236
0.1	0.2718	19.5865
0.2	0.5436	28.946
0.3	0.815	40.1379

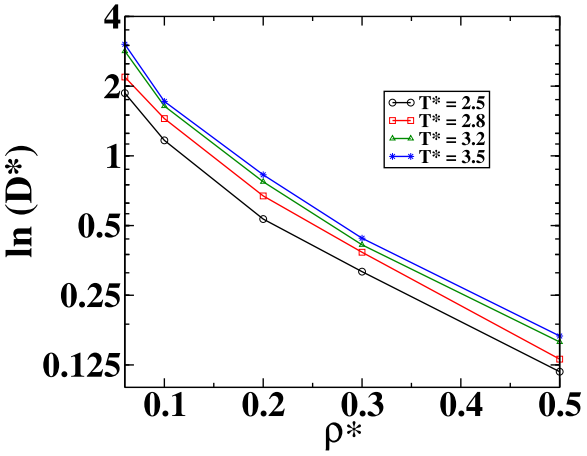

Fig. 5. The diffusion coefficient versus density for fixed temperatures.

observed in experiments [55–59]. The dependence on temperature for constant density (or pressure) illustrated in Fig. 6 is describe by an Arrhenius behavior

$$D \propto e^{\frac{-Ep}{RT}}, \tag{12}$$

where E_p is an activation energy and R is the molar gas constant. This is consistent with experimental results [55,56,58–60] and simulations [61–63] performed for more complex models. This qualitative agreement shows that our simple model is able to capture the mechanism for the mobility of the molecules. Our results suggest that the carbons are the responsible for the behavior of the mobility of the molecule and this is why our model is able to capture it.

Table 4 shows the values of activation energy obtained with our model and the experimental data (19.0 kJ/mol ($\rho = 1.8$ g/cm^3) [61], 13.3 kJ/mol [64], 12.7361 kJ/mol ($\rho = 0.9$ g/cm^3) [60] what suggests a good performance of the ab initio parametrization.

At high densities the Arrhenius diffusion coefficient gives rise to a non Arrhenius behavior illustrated in Fig. 7. At this low temperatures a fragile to strong transition is observed. This qualitative behavior confirms that our model is able to capture the glass phase for benzene. Some studies in literature observed the glass phase for benzene confined [65,66] and supercooled of benzene in mixtures with other liquids [67–70].

Next, we tested our model for describing the structure of the benzene. Fig. 8 illustrates the intermolecular carbon–carbon radial distribution (RDF) for four temperatures $T^* = 2.6$, 3.0, 4.5, and 5.0 a fixed density $\rho^* = 0.06$ for the benzene. The RDF was calculated with one site in one molecule with respect to one site of another molecule. No intramolecular RDF was computed. Since we want to observe the experimental peaks at the liquid phase, we do not include the RDF for high densities where the system approaches the glassy phase. Fig. 8 shows the three peaks which are experimentally observed [9,13]. We can separate the analysis in three regions: vicinity o the first, r^*_{first}, second, r^*_{second}, and third, r^*_{third}, peaks. At room temperature the experimental results indicate that the peaks height increases with the increasing distance. Atomistic simulations which do not parametrize the hydrogens are able to capture only two peaks, one between r_{first} and r_{second} and another at r_{third} [10,24]. Other more sophisticate computational approaches show the presence of the three peaks but they do not give the correct value or position. For instance, the OPLS-CS [12,14], OPLS [12] and OPT-FF [14] force fields give the correct location of the first peak but overestimate [12,14] but overestimate while the Rism underestimates its value [9]. The OPT-FF, AMBER03, GAFF, OPLS-AA, OPLS-CS, CHARMM27, GROMMOS [14] and TraPPe 9-sites and 6-sites [25] simulations models give a $g(r)$ for the second and third peaks larger than the experimental value while the AUA 9 and 6-sites give a RDF which is smaller than the experiments [25].

The relation between the three peaks and the benzene structure is not free from controversies in the literature. Both experimental results and simulations agree that at the liquid phase, the benzene forms clusters which decorrelated forming a "gas-like" cluster structure which can be observed by the smooth oscillations of the RDF after the first

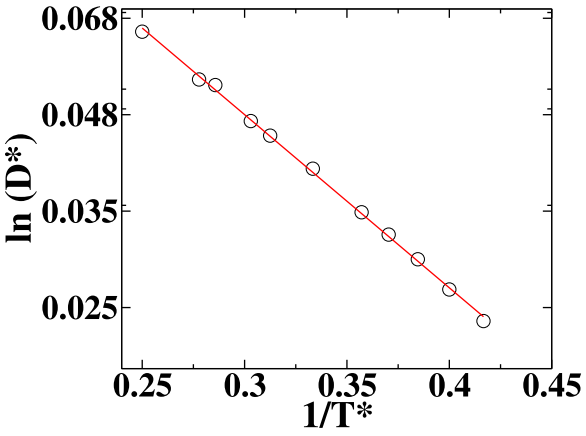

Fig. 6. The diffusion coefficient against the inverse of temperature for $\rho^* = 0.1$.

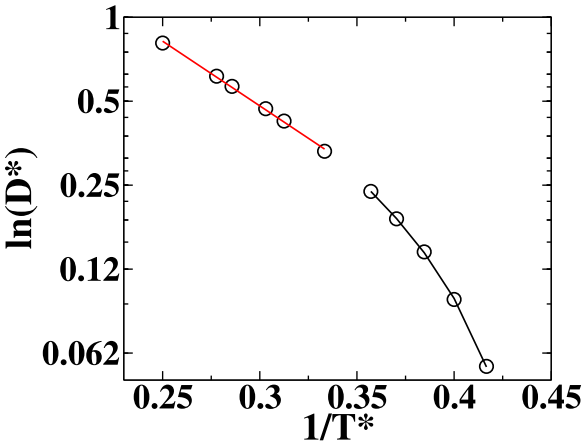

Fig. 7. The diffusion coefficient against the inverse of temperature for $\rho^* = 0.5$.

three peaks. Inside each cluster configuration which results in the three peaks has no consensus. Some simulations and experiments attribute the first peak at $r_{first} \approx 4$ Å to first neighbors dimer conformation to be face to face (also called parallel) [10,18,23], parallel displaced [10,12,14,21,24,71], while the third peak at 7 Å in both cases is attributed in all these cases to T-shaped or T-shaped displaced. The T-shaped is the predominant configuration [9] what is consistent with the large peak observed at 7 Å. Studies based in angular distribution proposes that at 4 Å the configuration is perpendicular and at 7 Å parallel [13]. Both experiments and simulations do not attribute any particular conformation to the second peak at 6 Å.

In our simulations we observed the three peaks. The first is located at $r_{min} \approx 4$ Å. Our radial distribution function accounts for one atom at each molecule. The conformations illustrated in Fig. 8 suggest that at this low distances the first neighbors molecules that at this short distance the configuration is parallel displaced. The second and third peaks are at larger distances when compared with the experimental results probably due to the way our RDF was computed removing averages over all atoms inside the molecule. The observed structure, however show T-shaped and T-shaped displaced at this second neighbor distances.

Finally, we computed the cluster size distribution versus number of cluster of molecules, n_c. The cluster size was analyzed based in the inter particle bonding [72,73]. Two molecules belong to the same cluster if the distance between them is smaller than 4.5σ, the in which the system becomes gas-like in Fig. 8. Since this method is sensitive to the choice of the cutoff parameter, we also tested smaller values and essentially the same result was obtained. The Fig. 9 illustrates probability $P(n_c/N)$ of finding a cluster with n_c molecules in N total number of molecules for a fixed density $\rho^* = 0.06$ which is the same density analyzed in Fig. 8. The cluster size distribution observed at $T^* = 2.6$ shows one clusters dominant around $n_c = 4$ what is consistent with the peak structure observed in Fig. 8. As the temperature is increased at $T^* = 4.5$ the cluster distribution becomes more broader with a peak at $n_c = 6$ and another at $n_c = 12$ what suggests that the temperature leads to a cluster percolation as observed in Fig. 8. The formation of clusters at the fluid phase is observed in works experimental [49,50] and simulations [10–12,51–54].

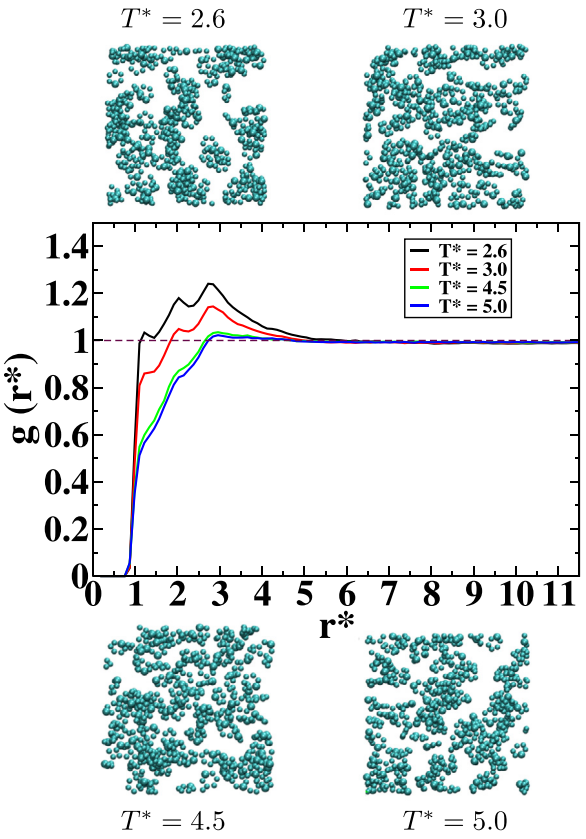

Fig. 8. Snapshots depicting the final configurations of the slab simulations for the benzene model (a) $T^* = 2.6$, (b) $T^* = 3.0$, (c) $T^* = 4.5$, and (d) $T^* = 5.0$. Carbon–carbon intermolecular pair distribution function for benzene computed with the new potential parameterized from ab initio calculations for temperatures $T^* = 2.6$–5.0 and density $\rho^* = 0.06$.

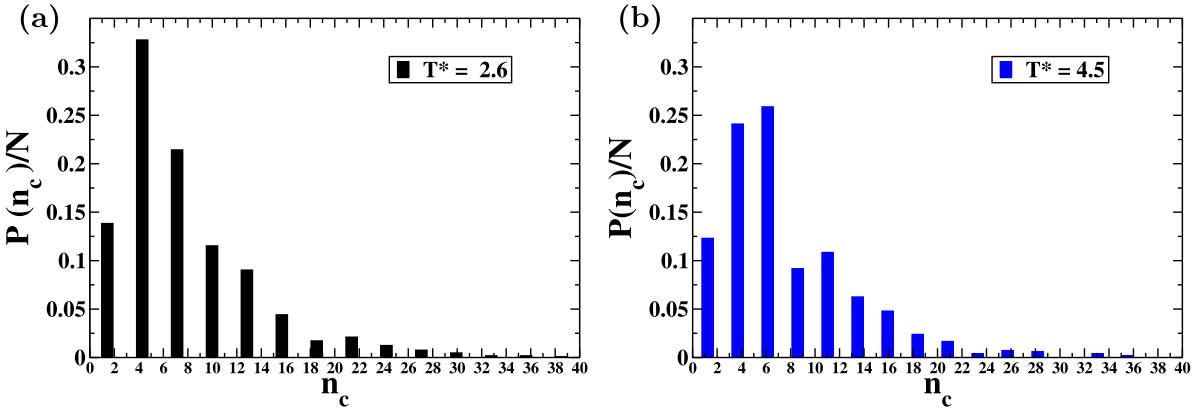

Fig. 9. Probability $P(n_c/N)$ of finding a cluster with size n_c versus n_c molecules for (a) $T^* = 2.6$, (b) $T^* = 4.5$, and density $\rho^* = 0.06$.

4. Conclusions

In this paper we explored the possibility of obtaining intermolecular potential starting from DFT energies. The idea behind the proposal is to construct potentials to be used in low temperature analysis where the quantum configurations might play a relevant role. This effective potentials do no aim to give correct energies for the system but to provide a view of the mechanism behind the processes. In order to test our analysis we developed a effective potential for benzene. Our analysis did no include the charge distribution in the molecule with the purpose of understanding what dynamic and

thermodynamic properties could be able to emerge from the carbon distribution. In this context the distance σ employed as unit of length measures the distance between sites which include the carbon and the hydrogen.

We obtained the diffusion coefficient for a number of temperature and our results are consistent with the experiments. Moreover for a range of temperatures the activation energies obtained from the diffusion versus inverse of temperature are quite close to the experimental values what suggests that for the dynamic processes the conformations and energies selected by the DFT were relevant for the mobility and the potential generated by them correctly captures the mechanism behind the molecular moves.

The RDF was also computed showing the three peaks characteristics of the experimental radial distribution function of the system. This result is quite surprising since the models which do not take the quadrupolar moments into account do not capture the three peaks. There is an on going debate about which conformations these three peaks represents. In our case visual inspection indicates that the first peaks relates to face to face or parallel slided, the second and the third, are related to T-shaped and T-shaped displaced configurations. These three conformations exhibit low energies at the DFT analysis.

We expect that this procedure would be useful for studying large molecules for which employing quantum analysis and temperature would be computational cost. In addition the use of effective models allow to understand which part of the interactions are responsible for the dynamics, structure and thermodynamics of the system.

Acknowledgments

The authors wish to acknowledge the financial support of the Brazilian Agencies CNPq, and CAPES. The Universidade Federal de Ouro Preto and Ronaldo Junio Campos Batista Grupo Nano (PROPP-UFOP), CENAPAD, INCT-FCx (CNPq/FAPESP) and BioMol (CAPES) for computational support. E.E.M. would like to thank Dr. George. G. Malenkov for helpful discussions.

References

[1] R. Fuentes-Azcatl, M.C. Barbosa, Thermodynamic and dynamic anomalous behavior in the tip4p/ε water model, Physica A 444 (2016) 86–94.
[2] R. Fuentes-Azcatl, M.C. Barbosa, Potassium bromide, kbr/ε: New force field, Physica A 491 (2018) 480–489.
[3] M. Minozzi, P. Gallo, M. Rovere, Supercooled water: A molecular dynamics simulation study with a polarizable potential, J. Mol. Liq. 127 (1–3) (2006) 28–32.
[4] M. Nguyen, S.W. Rick, The influence of polarizability and charge transfer on specific ion effects in the dynamics of aqueous salt solutions, J. Chem. Phys. 148 (2018) 222803.
[5] J.S. Kim, Z. Wu, A.R. Morrow, A. Yethiraj, A. Yethiraj, Self-diffusion and viscosity in electrolyte solutions, J. Phys. Chem. 116 (2012) 12007–12013.
[6] I. Cacelli, G. Cinacchi, G. Prampolini, A. Tani, Computer simulation of solid and liquid benzene with an atomistic interaction potential derived from ab initio calculations, J. Am. Chem. Soc. 126 (2004) 14278–14286.
[7] W. Kohn, L.J. Sham, Self-consistent equations including exchange and correlation effects, Phys. Rev. A 140 (1965) 1133.
[8] A. Barros de Oliveira, P.A. Netz, T. Colla, M.C. Barbosa, Thermodynamic and dynamic anomalies for a three-dimensional isotropic core-softened potential, J. Chem. Phys. 124 (2006) 084505.
[9] A. Narten, X-ray diffraction pattern and models of liquid benzene, J. Chem. Phys. 67 (1977) 2102–2108.
[10] M. Claessens, M. Ferrario, J.-P. Ryckaert, The structure of liquid benzene, Mol. Phys. 50 (1983) 217–227.
[11] P. Zorkii, E. Sokolov, L. Lanshina, G. Malenkov, Computer simulation of large clusters and quasi-periodic benzene models imitating the structure of the liquid phase, Russ. J. Phys. Chem. A 74 (2000) 1771–1776.
[12] C.M. Baker, G.H. Grant, The structure of liquid benzene, J. Chem. Theory Comput. 2 (2006) 947–955.
[13] M. Katayama, S. Ashiki, T. Amakasu, K. Ozutsumi, Liquid structure of benzene and its derivatives as studied by means of x-ray scattering, Phys. Chem. Liq. 48 (2010) 797–809.
[14] C.-F. Fu, S.X. Tian, A comparative study for molecular dynamics simulations of liquid benzene, J. Chem. Theory Comput. 7 (2011) 2240–2252.
[15] K. Yoshida, N. Fukuyama, T. Yamaguchi, S. Hosokawa, H. Uchiyama, S. Tsutsui, A.Q. Baron, Inelastic x-ray scattering on liquid benzene analyzed using a generalized langevin equation, Chem. Phys. Lett. 680 (2017) 1–5.
[16] T. Sato, T. Tsuneda, K. Hirao, A density-functional study on π-aromatic interaction: Benzene dimer and naphthalene dimer, J. Chem. Phys. 123 (2005) 104307.
[17] T. Bogdan, Atom-atomic potentials and the correlation distribution functions for modeling liquid benzene by the molecular dynamics methods, Russ. J. Phys. Chem. A 80 (2006) S14–S20.
[18] G. Prampolini, P.R. Livotto, I. Cacelli, Accuracy of quantum mechanically derived force-fields parameterized from dispersion-corrected dft data: the benzene dimer as a pprototype for aromatic interactions, J. Chem. Theory Comput. 11 (2015) 5182–5196.
[19] M.I. Cabaço, Y. Danten, M. Besnard, Y. Guissani, B. Guillot, Neutron diffraction and molecular dynamics study of liquid benzene and its fluorinated derivatives as a function of temperature, J. Phys. Chem B 101 (1997) 6977–6987.
[20] M. Misawa, T. Fukunaga, Structure of liquid benzene and naphthalene studied by pulsed neutron total scattering, J. Chem. Phys. 93 (1990) 3495–3502.
[21] T.F. Headen, C.A. Howard, N.T. Skipper, M.A. Wilkinson, D.T. Bowron, A.K. Soper, Structure of π- π interactions in aromatic liquids, J. Am. Chem. Soc. 132 (2010) 5735–5742.
[22] F. Adan, A. Banon, J. Santamaria, A monte carlo study of liquid benzene, Chem. Phys. 86 (1984) 433–444.
[23] W.L. Jorgensen, D.L. Severance, Aromatic-aromatic interactions: free energy profiles for the benzene dimer in water, chloroform, and liquid benzene, J. Am. Chem. Soc. 112 (1990) 4768–4774.
[24] K. Coutinho, S. Canuto, M. Zerner, CaLculation of the absorption spectrum of benzene in condensed phase. a study of the solvent effects, Int. J. Quantum Chem. 65 (1997) 885–891.
[25] P. Bonnaud, C. Nieto-Draghi, P. Ungerer, Anisotropic united atom model including the electrostatic interactions of benzene, J. Phys. Chem B 111 (2007) 3730–3741.
[26] P. Hohenberg, Inhomogeneous electron gas, Phys. Rev. B 136 (1964) 864.
[27] W. Kohn, Self-consistent equations including exchange and correlation effects, Phys. Rev. A 140 (1965) 1133.

[28] E.E. Moraes, M.D. Coutinho-Filho, R.J. Batista, Transport properties of hydrogenated cubic boron nitride nanofilms with gold electrodes from density functional theory, ACS Omega 2 (2017) 1696–1701.
[29] J.M. Soler, E. Artacho, J.D. Gale, A. García, J. Junquera, P. Ordejón, D. Sánchez-Portal, The siesta method for ab initio order-n materials simulation, J. Phys.: Condens. Matter 14 (2002) 2745.
[30] J.P. Perdew, A. Zunger, Self-interaction correction to density-functional approximations for many-electron systems, Phys. Rev. B 23 (1981) 5048.
[31] S.F. Boys, F.d. Bernardi, The calculation of small molecular interactions by the differences of separate total energies. some procedures with reduced errors, Mol. Phys. 19 (1970) 553–566.
[32] J.P. Perdew, K. Burke, M. Ernzerhof, Generalized gradient approximation made simple, Phys. Rev. Lett. 77 (1996) 3865.
[33] E. Artacho, E. Anglada, O. Diéguez, J.D. Gale, A. García, J. Junquera, R.M. Martin, P. Ordejón, J.M. Pruneda, D. Sánchez-Portal, et al., The siesta method; developments and applicability, J. Phys.: Condens. Matter 20 (2008) 064208.
[34] L. Kong, G. Román-Pérez, J.M. Soler, D.C. Langreth, Energetics and dynamics of h 2 adsorbed in a nanoporous material at low temperature, Phys. Rev. Lett. 103 (2009) 096103.
[35] F. Tournus, J.-C. Charlier, Ab initio study of benzene adsorption on carbon nanotubes, Phys. Rev. B 71 (2005) 165421.
[36] S.D. Chakarova-Käck, E. Schröder, B.I. Lundqvist, D.C. Langreth, Application of van der waals density functional to an extended system: adsorption of benzene and naphthalene on graphite, Phys. Rev. Lett. 96 (2006) 146107.
[37] J. Ma, L.-W. Wang, Using wannier functions to improve solid band gap predictions in density functional theory, Sci. Rep. 6 (2016) 24924.
[38] X. Li, S. Zhang, C. Zhang, Q. Wang, Stabilizing benzene-like planar n 6 rings to form a single atomic honeycomb ben 3 sheet with high carrier mobility, Nanosc 10 (2018) 949–957.
[39] M.P. Allen, D.J. Tildesley, Computer Simulation of Liquids, Oxford university press, 2017.
[40] I. Cacelli, G. Cinacchi, G. Prampolini, A. Tani, Computer simulation of solid and liquid benzene with an atomistic interaction potential derived from ab initio calculations, J. Am. Chem. Soc. 126 (2004) 14278–14286.
[41] C. Amovilli, I. Cacelli, G. Cinacchi, L. De Gaetani, G. Prampolini, A. Tani, Structure and dynamics of mesogens using intermolecular potentials derived from ab initio calculations, Theor. Chem. Acc. 117 (2007) 885–901.
[42] I. Cacelli, A. Cimoli, P.R. Livotto, G. Prampolini, An automated approach for the parameterization of accurate intermolecular force-fields: Pyridine as a case study, J. Comput. Chem. 33 (2012) 1055–1067.
[43] K.J. Millman, M. Aivazis, Python for scientists and engineers, Comput. Sci. Eng. 13 (2011) 9–12.
[44] S. van der Walt, S.C. Colbert, G. Varoquaux, The numpy array: a structure for efficient numerical omputation, Comput. Sci. Eng. 13 (2011) 22–30.
[45] S. Plimpton, P. Crozier, A. Thompson, Lammps-large-scale atomic/molecular massively parallel simulator, Sandia Natl. Lab. 18 (2007) 43.
[46] W.G. Hoover, Canonical dynamics: equilibrium phase-space distributions, Phys. Rev. A 31 (1985) 1695.
[47] W.G. Hoover, Constant-pressure equations of motion, Phys. Rev. A 34 (1986) 2499.
[48] M.O. Sinnokrot, C.D. Sherrill, Unexpected substituent effects in face-to-face π-stacking interactions, J. Phys. Chem. A 107 (2003) 8377–8379.
[49] D.C. Easter, R.L. Whetten, J.E. Wessel, Spectroscopic evidence for high symmetry in (benzene) 13, J. Chem. Phys. 94 (1991) 3347–3354.
[50] D.C. Easter, A. Baronavski, M. Hawley, A spectroscopic investigation of the nonrigid–rigid transition of (benzene) 13 during free jet expansion, J. Chem. Phys. 99 (1993) 4942–4951.
[51] H. Takeuchi, Structural features of small benzene clusters $(c_6h_6)_n$ ($n \leq 30$) as investigated with the all-atom opls potential, J. Phys. Chem. A 116 (2012) 10172–10181.
[52] D.C. Easter, Low-energy structures of (c6h6) 13 as determined by low-tempecrature monte carlo simulations using several potential energy surfaces, J. Phys. Chem. A 107 (2003) 2148–2159.
[53] J. Marques, F. Pereira, J. Llanio-Trujillo, P. Abreu, M. Albertí, A. Aguilar, F. Pirani, M. Bartolomei, A global optimization perspective on molecular clusters, Phil. Trans. R. Soc. A 375 (2017) 20160198.
[54] W. Gao, J. Jiao, H. Feng, X. Xuan, L. Chen, From clusters to liquid: what are the preferred ways for benzene and pyrrole to interact?, Theor. Chem. Acc. 132 (2013) 1340.
[55] K. Tanabe, Raman study of reorientational motion of liquid benzene, Chem. Phys. 31 (1978) 319–325.
[56] K. Yoshida, N. Matubayasi, Y. Uosaki, M. Nakahara, Self-diffusion in supercritical water and benzene in high-temperature high-pressure conditions studied by nmr and dynamic solvation-shell model, J. Phys.: Conf. Ser. 215 (2010) 012093.
[57] M. McCool, A. Collings, L. Woolf, Pressure and temperature dependence of the self-diffusion of benzene, J. Chem. Soc. Faraday Trans. 68 (1972) 1489–1497.
[58] H. Parkhurst Jr, J. Jonas, Dense liquids. i. the effect of density and temperature on self-diffusion of tetramethylsilane and benzene-d 6, J. Chem. Phys. 63 (1975) 2698–2704.
[59] M. Brüsewitz, A. Weiss, Pressure-temperature-dependence of mass density and self-diffusion coefficients in the binary liquid system n-hexane/benzene, Ber. Bunsenges. Phys. Chem. 94 (1990) 386–391.
[60] H. Hiraoka, J. Osugi, W. Jono, Self-diffusion of benzene and diffusions of sulfur and iodine in benzene under pressure, Rev. Phys. Chem. Japan. 28 (1958) 54–60.
[61] M. Schwartz, D. Duan, R. Berry, Molecular dynamics study of anisotropic translational and rotational diffusion in liquid benzene, J. Phys. Chem. 109 (2005) 8637–8641.
[62] W.G. Rothschild, Revisit of rotational motion of axial poly-atomics by molecular dynamics simulation and group theory: liquid benzene at 298, 365, 432, 498, 562 k, Mol. Phys. 110 (2012) 2269–2273.
[63] H. Mohammadi-Manesh, S. Tashakor, S. Alavi, Diffusion of benzene through the beta zeolite phase, Micropor. Mesopor. Mat. 181 (2013) 29–37.
[64] R. Witt, L. Sturz, A. Dölle, F. Müller-Plathe, Molecular dynamics of benzene in neat liquid and a solution containing polystyrene. 13c nuclear magnetic relaxation and molecular dynamics simulation results, J. Phys. Chem. 104 (2000) 5716–5725.
[65] C. Alba-Simionesco, G. Dosseh, E. Dumont, B. Frick, B. Geil, D. Morineau, V. Teboul, Y. Xia, Confinement of molecular liquids: Consequences on thermodynamic, static and dynamical properties of benzene and toluene, Eur. Phys. J. 12 (2003) 19–28.
[66] Y. Xia, G. Dosseh, D. Morineau, C. Alba-Simionesco, Phase diagram and glass transition of confined benzene, J. Phys. Chem. 110 (2006) 19735–19744.
[67] S.F. Swallen, P.A. Bonvallet, R.J. McMahon, M. Ediger, Self-diffusion of tris-naphthylbenzene near the glass transition temperature, Phys. Rev. Lett. 90 (2003) 015901.
[68] C. Angell, Glass-formers and viscous liquid slowdown since david turnbull: enduring puzzles and new twists, MRS Bull. 33 (2008) 544–555.
[69] R.A. May, R.S. Smith, B.D. Kay, Mobility of supercooled liquid toluene, ethylbenzene, and benzene near their glass transition temperatures investigated using inert gas permeation, J. Phys. Chem. A 117 (2013) 11881–11889.
[70] W. Tu, Z. Chen, X. Li, Y. Gao, R. Liu, L.-M. Wang, Revisiting the glass transition and dynamics of supercooled benzene by calorimetric studies, J. Chem. Phys. 143 (2015) 164501.
[71] C. Nieto-Draghi, P. Bonnaud, P. Ungerer, Anisotropic united atom model including the electrostatic interactions of methylbenzenes. i. thermodynamic and structural properties, J. Phys. Chem. C 111 (2007) 15686–15699.
[72] J.C.F. Toledano, F. Sciortino, E. Zaccarelli, Colloidal systems with competing interactions: from an arrested repulsive cluster phase to a gel, Soft Matter 5 (12) (2009) 2390–2398.
[73] J.R. Bordin, Distinct aggregation patterns and fluid porous phase in a 2d model for colloids with competitive interactions, Physica A 495 (2018) 215–224.